Epitaxial growth of $(FeCo)_xGe_{1-x}(001)$

L. He, B. A. Collins, and F. Tsui[a)]
Department of Physics and Astronomy, University of North Carolina, Chapel Hill, North Carolina 27599-3255

Y. Zhong, S. Vogt, and Y. S. Chu
Advanced Photon Source, Argonne National Laboratory, Argonne, Illinois 60439

(Received 6 November 2006; accepted 14 May 2007; published 25 June 2007)

The epitaxial growth of $(FeCo)_xGe_{1-x}$ films on Ge and GaAs (001) substrates has been studied systematically with x in the range between 0 and 17 at. %, using combinatorial molecular beam epitaxy (MBE) techniques. Complementary doping using the two transition metal dopants into Ge (001) during MBE growth is shown to produce high quality coherent epitaxial films for transition metal concentrations as high as 11 at. %. As the doping level increases, rough growth occurs, which is accompanied by an increasing amount of stacking faults along the ⟨111⟩ directions. The crystal lattice that resulted from the rough growth exhibits a large out-of-plane tetragonal distortion. There are no detectable secondary phases up to a combined transition metal concentration of 17 at. %. The behaviors are shown to be invariant with respect to the choice of substrates. © *2007 American Vacuum Society.* [DOI: 10.1116/1.2748409]

I. INTRODUCTION

Group IV based doped magnetic semiconductors have attracted a lot of attention, owing in part to their potential as the material candidates for the science and applications of spintronics[1] and their potential compatibility with Si-based processing technology. To date, many transition metal dopants have been used successfully to dope Ge during epitaxial growth, including the use of single and double dopants of Mn,[2] Cr,[3] Co,[4] Co and Mn,[5,6] and Fe and Mn.[7] While these systems show varying degrees of promising electronic and magnetic behaviors, there is a lack of fundamental understanding of the epitaxial growth processes and spin dependent states in these systems, such that structures and properties in these systems are yet to be controlled. This gives impetus to extensive investigations into these and related material systems.

In this article we report a study of the epitaxial growth and structural properties in a type of doped Ge magnetic semiconductor using Fe and Co as the codopants. The dependences on doping concentration and epitaxial constraints have been examined using combinatorial molecular beam epitaxy (MBE) techniques and by the use of two different substrates, Ge (001) and GaAs (001), owing to the 0.07% mismatch between the two lattices. A previous study[6] indicates that complementary doping into Ge (001) using Co and Mn with their respective atomic radii that are smaller and larger than Ge can compensate for the internal stress caused by the doping species. This method can stabilize the coherent epitaxial growth at higher doping levels than the system with a single dopant, leading to ferromagnetism near room temperature.[5] In the current study the larger dopant Mn has been replaced by Fe. An atomic ratio between the two codopants of approximately 1:1 was chosen based on their expected atomic radii in order to compensate for the respective strain effects in Ge lattice. The MBE growth and stabilizing high level of transition metal dopants are the focus of this article. In a separate article magnetic and magnetotransport phenomena of the films and the prospect of high temperature ferromagnetism in this material system will be reported.

II. EXPERIMENT

Synthesis was carried out in an advanced combinatorial MBE system. The Ge (001) and GaAs (001) substrates were first cleaned using the standard RCA method. They were then mounted side by side onto a Mo sample holder and subsequently loaded into the growth chamber. Preceding the growth they were first degassed at 600 °C for about 20 min under UHV conditions. A thin Ge buffer layer (typically 50 Å thick) was grown at 250 °C and then annealed at 600 °C (for up to 20 min). This growth-anneal cycle was repeated several times resulting in a combined buffer layer of 380 Å thick, in order to produce an atomically flat Ge (001) surface across each substrate. The specific growth-anneal cycle was developed for preparing Ge buffer layers on Ge substrates,[6] and since the parameters used are comparable to those for MBE growth of Ge/GaAs superlattices,[8,9] it was also employed for this study in order to keep the conditions identical for the two substrates. However, subsequent secondary ion mass-spectrometry (SIMS) analysis indicates the presence of excess Ga in Ge (<0.01 at. %), and thus the parameters used for preparing the buffer layer on GaAs may be less than optimal.

For the growth of doped films, we employed a multilayer approach by sequential deposition of Ge–Co–Ge–Fe layers. This was combined with precision shadow masks, pneumatic source shutters, and real-time atomic absorption spectroscopy flux monitors to control the doping profiles of the two dopants across the substrates. Ge was doped at an interval of

[a)]Electronic mail: ftsui@physics.unc.edu

2 Å alternately by depositing nearly identical submonolayer wedges of Fe and Co, thus producing the so-called binary combinatorial sample $(FeCo)_xGe_{1-x}$ with a range of combined doping concentration x between 0 and 17 at. % over a distance of 10 mm. The film thickness changes from 910 to 1010±10 Å, as the transition metal concentration increases from 0 to 10 at. %, which is confirmed by x-ray diffraction (XRD) analysis. Composition and thickness-dependent structural properties were probed in real time by scanning reflection high-energy electron diffraction (RHEED). The film growth was terminated (at ~1000 Å) when the thickness dependence was determined to be fully saturated. Electron-beam hearths were used to evaporate the three elements, and the growth temperature and rate were 250 °C and ~0.1 Å/s, respectively. Detailed descriptions of the combinatorial MBE synthesis are published elsewhere.[10,11]

X-ray microbeam techniques[12,13] were used to characterize the structure and composition of the two combinatorial samples. Both microbeam XRD and x-ray fluorescence (XRF) spectroscopy experiments were carried out at the 2–BM beamline of the Advanced Photon Source (APS) in Argonne National Laboratory. Kirkpatrick-Baez (KB) mirrors were used to produce a focused x-ray beam with a spot size of 10 μm in lateral dimensions, resulting in a maximum composition spread of ~0.02 at. % within the beam. The atomic ratio between Fe and Co has been determined to be 1.00:1.17 by the XRF measurements. In addition to a point detector, an area detector (CCD) was also used for wide-angle XRD experiments. The area detector allows the simultaneous detection of scattering intensities within a relatively large region of reciprocal space. This provides an efficient way to detect and quantify weak powder intensities from trace amounts of secondary phases and weak intensities from certain types of defects, such as stacking faults.

III. RESULTS AND DISCUSSIONS

Under the conditions outlined above, the growth of $(FeCo)_xGe_{1-x}$ at doping levels (x) below a thickness-dependent threshold is coherent and smooth layer by layer, and at higher doping levels the growth front becomes three dimensional (3D) while the growth remains epitaxial up to $x \sim 17$ at. %, as shown in Fig. 1 by the RHEED analysis for the behavior at ~1000 Å. The thickness-dependent threshold decreases as the coverage increases, and saturates above several hundred angstroms to ~11 at. %. The behavior is similar to the one reported previously for Co and Mn codoped Ge (001),[6] and it is found to be invariant with respect to the two substrates Ge (001) and GaAs (001).

At low doping concentrations, RHEED patterns indicate atomically smooth two-dimensional (2D) surfaces with 2×1 surface reconstructions, as shown in Fig. 1(a), and exhibit intensity oscillations during growth. At ~1000 Å of coverage, the specular intensity [the arrow in Fig. 1(a)] remains high up to a concentration of 11 at. % [open circles in Fig. 1(d)], where a roughening transition occurs. Within a narrow range around the transition, the RHEED specular intensities and 2×1 surface reconstruction patterns vanish [Figs. 1(d) and 1(e)], while 3D transmission-like features (rather than reflection) with modulated streak patterns appear [Fig. 1(b)]. The diffraction conditions were set intentionally with the specular position placed at the so-called "anti-Bragg" position, such that the corresponding peak position perpendicular to the surface ($q_\perp$) exhibits a jump at the roughening transition [Fig. 1(e)].

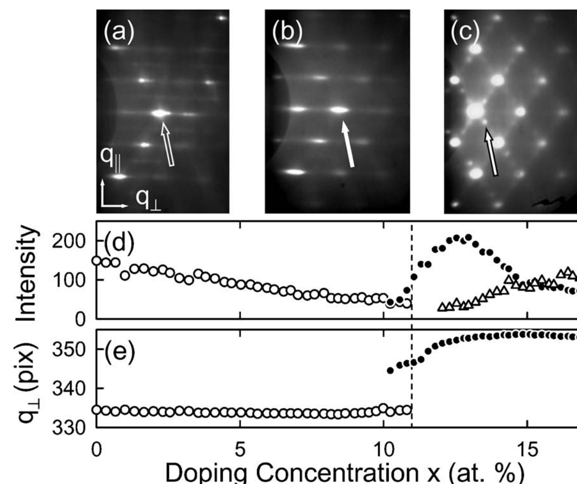

FIG. 1. Evolution of RHEED patterns of a $(FeCo)_xGe_{1-x}$ combinatorial sample grown on GaAs (001). [(a)–(c)] RHEED patterns along the [110] azimuth (vertical) at different doping concentrations: $x \sim 5$ at. % (a), ~11 at. % (b), and ~16 at. % (c). The in-plane [110] and out-of-plane [001] directions are indicated by the arrows and the respective $q_\parallel$ and $q_\perp$ in (a). The satellite spots between the bright Bragg reflections in (c) correspond to stacking faults along the ⟨111⟩ directions. [(d) and (e)] RHEED peak intensity (in arbitrary units) and position along the [001] direction $q_\perp$ (in pixels). The open and closed circles and triangles correspond to the parameters for the 2D specular reflection [the arrow in (a)], the 3D Bragg reflection [the arrow in (b)], and the stacking fault peak [the arrow in (c)], respectively. The vertical dashed line indicates the transition from the 2D coherent epitaxial growth to the 3D rough growth.

At larger x, the specular intensity disappears completely and the RHEED patterns become spotty, with bright Bragg spots accompanied by satellite peaks along the ⟨111⟩ directions [Fig. 1(c)]. The slightly weaker satellite peaks have been identified to be from the stacking faults along the ⟨111⟩ directions. Specifically, these intensities arise from the twinned family of {022} reflections rotated 60° around one of the ⟨111⟩ directions. The onset of the intensities appears to coincide with that of the roughening transition [Fig. 1(d)]. This has been confirmed by the wide-angle XRD measurements using an area detector (CCD), as discussed below (Fig. 3). The rough growth evidently exposes the {111} planes that are prone to the formation of the sixfold stacking faults.[14,15] It is interesting to note that the behavior is similar to those observed in the low temperature homoepitaxial growth of Si and Ge (Refs. 14 and 15) with a significantly lower temperature than the current system, suggesting similar underlying processes. It is reasonable to expect that the presence of dopants can kinetically change the diffusion processes and thus significantly lower the effective growth temperature.

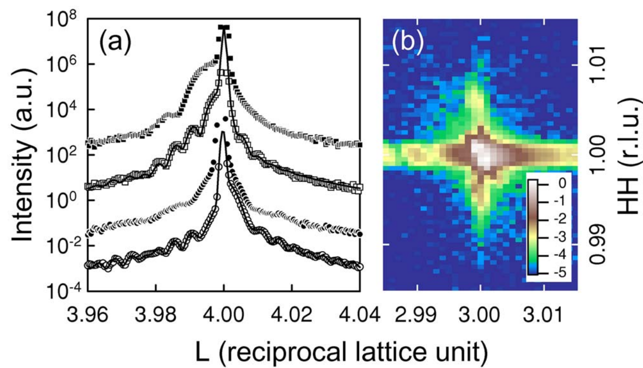

FIG. 2. (a) X-ray diffraction intensities along [00L] through the Ge (004) reflection for two $(FeCo)_xGe_{1-x}(001)$ combinatorial samples at different doping concentrations. 2D coherent films exhibit XRD fringes (open symbols), which are absent in 3D rough films (solid symbols). The circle and square symbols correspond to films grown on Ge (001) and GaAs (001) substrates, respectively. The lines are fits using a simple kinematical model. For clarity the curves are shifted vertically from each other by two decades. (b) High resolution reciprocal map around the (113) reflection for a $[FeCo]_xGe_{1-x}(001)$ sample at $x\sim 8$ at. %. The numbers in the legend for the intensity corresponds to the exponent of the base 10 logarithmic scale. The coherent truncation rod with intensity oscillations (for $L<3$) along the [11L] direction is clearly shown. The width across L=3.01, i.e., [1,1,3.01] corresponds to instrument resolution.

The coherent epitaxial growth and the presence of a composition-dependent roughening transition are also confirmed by XRD experiments, as shown in Fig. 2. At low doping concentrations, the XRD intensities [open symbols in Fig. 2(a)] exhibit fringe patterns on either side of the (004) Bragg reflection, dominated by the intensity from the substrate. The fringes arise from the interference of the x rays scattered from the film, the substrate, and the associated 2D surface and interfaces. They disappear when the surface becomes rough [closed symbols in Fig. 2(a), i.e., the third curve from the top]. A typical high resolution XRD reciprocal map around the (113) Bragg reflection within the 2D growth regime is also shown in Fig. 2(b). The sharp truncation rod with coherent fringes along the out-of-plane [00L] direction proves unequivocally that the film is coherent with respect to the substrate. The width [along the in-plane HH direction, vertical in Fig. 2(b)] of the truncation rod away from the (113) reflection of the substrate is that of the instrument resolution.

Within the 2D growth regime, the phase shift of the scattering amplitude in reciprocal space and the resulting asymmetry in the intensity of the fringe patterns are directly related to the out-of-plane lattice strain between the film and the substrate, which can be determined by fitting the XRD pattern using a simple kinematical model [lines in Fig. 2(a)]. As shown in Fig. 2(a), the zeroth order fringe for the film grown on Ge (circles) is shifted to a higher value in reciprocal space (the shoulder on the right), indicating that the out of plane lattice constant of the film is smaller than that of the Ge substrate. In contrast the counterpart grown on GaAs (squares) is shifted to a lower value (the shoulder on the left), indicating a larger lattice constant than that of the GaAs substrate. The former corresponds to an out-of-plane compression, while the latter corresponds to a tensile strain out of plane. Despite of having opposite strain states, the two films exhibit the same roughening transition at the same doping concentration. This finding indicates that the observed transition is an intrinsic composition driven phenomenon.

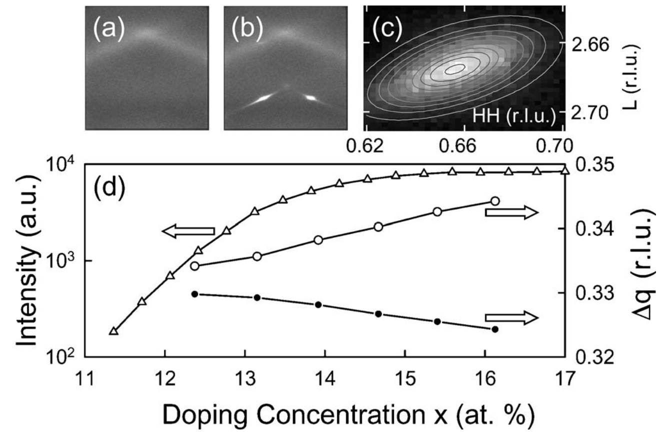

FIG. 3. Evolution of the intensity and position of the stacking fault peak for a $(FeCo)_xGe_{1-x}(001)$ combinatorial sample grown on Ge (001). [(a) and (b)] XRD intensities detected by an area detector (CCD) for $x\sim 8$ and 15 at. %, respectively. The area detector is positioned approximately perpendicular to the [110] direction with the vertical axis along the [00L] direction. The broad intensities near the top of the images are the thermal diffused scattering from the substrate, and the sharp spots are the stacking fault peaks. (c) A high resolution reciprocal map around the (2/3, 2/3, 8/3) stacking fault peak using a point detector. The elliptical lines are from a 2D Gaussian fit. (d) The integrated intensity (triangle) of the stacking fault peak [Fig. 3(b)] as a function of the doping concentration. The in-plane (HH) and out-of-plane (L) peak positions in reciprocal space of the stacking fault, as expressed in the differences in reciprocal space (Δq) between the positions of the high resolution stacking fault peak [Fig. 3(c)] and the nearest Bragg reflection: Δq=3-L for the out-of-plane (L) direction (closed circles) and Δq=1-HH for the in-plane (HH) direction (open circles). The crystal lattice in the 3D regime exhibits a very large tetragonal distortion along the growth direction.

The evolution of the stacking faults and the possible presence of powder intensities have been examined by XRD using an area detector and using high resolution 2D reciprocal mapping with a point detector, as shown in Fig. 3. As described above, we use the area detector to detect the secondary phase and to quantify the intensities of stacking faults and the reciprocal mapping for quantifying the positions of the diffraction peaks. As shown in Figs. 3(a) and 3(b), intensities within the 2D regime are nearly featureless, while 3D counterparts show stacking fault peaks. There are no detectable intensities from secondary phases, whose maximum volume fraction has been estimated to be about 0.5%–1%. In the next paragraph we discuss how this estimate is made.

In general, it is quite difficult to place a lower detection limit for XRD because the intensity of the diffracted beam over a fixed detection solid angle depends on the specific crystalline details of the secondary phases. If the secondary phases precipitate into large size ($\sim\mu$m) grains, the diffracted beam would be highly collimated over a narrow solid angle and could be detected with high detection sensitivity. In contrast if the secondary phases are amorphous, no measurable diffraction can be obtained. A recent synchrotron study,[16] carried out using the same beamline at APS (2–BM),

demonstrates that second-phase particles of $Zr(Fe_{1.5}Cr_{0.5})_2$ within a polycrystalline Zr matrix, with 0.24 wt % of Fe and 0.11 wt % of Cr, can be measured well above the detection limit. The work was performed under considerable scattering background from the Zr matrix and by detecting the weaker scatterers in the secondary phase, i.e., Fe and Cr that scatter ~2.5 times less than Zr. In the current study, while the single crystal Ge substrate does not contribute to any background intensity that hinders the detection of possible secondary phases, the small sample thickness would reduce the total integrated intensity from the secondary phases. Based on these, a conservative estimate for minimum detection level has been made as stated above, which is also equivalent to a Fe or Co film of about 5 to 10 Å thick.

The integrated intensity of the stacking fault peak exhibits an exponential decrease as the doping concentration decreases from 17 at. % towards the roughening transition of ~11 at.%, as shown in the triangles in Fig. 3(d). This confirms the RHEED analysis discussed above [triangles in Fig. 1(d)], such that the appearance of stacking faults coincides with the onset of the 3D rough growth. The stacking fault peaks as measured by the high resolution reciprocal mapping [Fig. 3(c)] have been fit using a 2D Gaussian function [elliptical contours in Fig. 3(c)]. From the fit the in-plane (HH) and out-of-plane (L) peak positions in reciprocal space of the stacking fault have been determined. The results are shown in Fig. 3(d), as they are expressed in the position of the stacking fault peak from that of the (113) reflection of the substrate. The lattice associated with the stacking faults appears to exhibit a very large tetragonal distortion along the growth direction, and the distortion increases monotonically with doping concentration. Such a large effect does not appear to be consistent with effects associated with the strain relaxation process and differential thermal expansions, and therefore, further studies are needed to elucidate this.

Finally the observed doping concentration dependent behaviors are qualitatively the same as those observed in the epitaxial growth of Co and Mn codoped Ge (001).[6] This finding indicates that the MBE growth processes in the two systems may be influenced by similar mechanisms.

IV. SUMMARY

We have shown that high quality coherent epitaxial films of $(FeCo)_xGe_{1-x}$ (001) can be synthesized for transition metal concentrations as high as 11 at. %. Rough disordered growth occurs at higher concentrations, which is accompanied by stacking faults along the ⟨111⟩ directions without any detectable secondary phases for doping levels as high as 17 at. %. The structure of the film exhibits systematic changes as a function of the transition metal concentration, and the lattice associated with the stacking faults in the 3D growth regime exhibits a large out-of-plane tetragonal distortion.

ACKNOWLEDGMENTS

The authors wish to thank W. Rice, M. Wolboldt, and P. Muduli for assistance and discussions. The work is supported in part by NSF DMR-0441218 for MBE synthesis, by DOD W911NF-05-1-0173 for MBE instrumentation, and by DOE BES DE-FG02-05ER46216 for the measurements and student support (B.A.C. and L.H.). An APS subcontract 5F-00428 for the partial student support is also acknowledged. The use of the Advanced Photon Source is supported by the U. S. Department of Energy, Office of Sciences, Office of Basic Energy Sciences, under Contract No. DE-AC02-06CH11357.

[1]G. A. Prinz, Phys. Today **48**(4), 58 (1995).
[2]Y. D. Park *et al.*, Science **295**, 651 (2002).
[3]S. Choi *et al.*, Appl. Phys. Lett. **81**, 3606 (2002).
[4]V. Ko, K. L. Teo, T. Liew, and T. C. Chong, Appl. Phys. Lett. **89**, 042504 (2006).
[5]F. Tsui, L. He, L. Ma, A. Tkachuk, Y. S. Chu, K. Nakajima, and T. Chikyow, Phys. Rev. Lett. **91**, 177203 (2003).
[6]F. Tsui, L. He, A. Tkachuk, S. Vogt, and Y. S. Chu, Phys. Rev. B **69**, 081304R (2004).
[7]R. R. Gareev *et al.*, Appl. Phys. Lett. **88**, 222508 (2006).
[8]C. A. Chang, A. Segmüller, L. L. Chang, and L. Esaki, Appl. Phys. Lett. **38**, 912 (1981).
[9]C. A. Chang and T. S. Kuan, J. Vac. Sci. Technol. A **1**, 315 (1983).
[10]Y. K. Yoo and F. Tsui, MRS Bull. **27**, 316 (2002).
[11]F. Tsui and L. He, Rev. Sci. Instrum. **76**, 062206 (2005).
[12]Y. S. Chu *et al.*, Appl. Surf. Sci. **223**, 175 (2004).
[13]S. Vogt, Y. S. Chu, A. Tkachuk, P. Ilinski, D. Walko, and F. Tsui, Appl. Surf. Sci. **223**, 214 (2004).
[14]D. J. Eaglesham, A. E. White, L. C. Feldman, N. Moriya, and D. C. Jacobson, Phys. Rev. Lett. **70**, 1643 (1993).
[15]O. P. Karpenko, S. M. Yalisove, and D. J. Eaglesham, J. Appl. Phys. **82**, 1157 (1997).
[16]K. T. Erwin, O. Delaire, A. T. Motta, Y. S. Chu, D. C. Mancini, and R. C. Birtcher, J. Nucl. Mater. **294**, 299 (2001).